Stability of Load Bearing Trapezoidal Diaphragms

Stabilité d'entretoises trapézoidales sous charges

Stabilität trapezförmiger belasteter Querträger

K. C. ROCKEY
M.Sc., Ph.D., C.Eng., F.I.C.E., M.I. Mech.E. Professor of Civil and Structural Engineering, University College, Cardiff, U.K.

M. A. EL-GAALY
M.S.E., D.Sc., M.ASCE
Research Fellow, Civil and Structural Engineering Department, University College, Cardiff, U.K.

1. Introduction

In box girders, diaphragms are employed to transfer the vertical shear force carried by the webs to the supports. The stress distribution which occurs in load bearing diaphragms is complex and varies with the inclination of the webs and the position of the bearing pads. In order to be able to design such diaphragms it is necessary to know the loads at which the diaphragm will buckle either locally or in an overall mode. A survey of the existing literature shows that little information is available regarding the overall buckling of trapezoidal diaphragms.

A finite element study has therefore been carried out to determine the stress distribution which occurs in both rectangular and trapezoidal diaphragms and to determine the applied load at which overall buckling of the diaphragms will occur. In the present paper the overall buckling load of unstiffened trapezoidal and rectangular diaphragms has been determined for different geometric properties of the diaphragms and for varying position and length of the supporting pads. It is fully appreciated that most large diaphragms are stiffened and in a forthcoming paper, the buckling of orthogonally stiffened diaphragms will be dealt with.

2. Method of Analysis

Since the finite element method of analysis which has been used in the present study has been reported elsewhere [1]–[4] full details of the method

will not be given here. In the present study a constant strain plane stress triangular element having 6 degrees of freedom [1], [5], [6], [7] was used to evaluate the inplane stresses, and in the buckling analysis a non-conforming triangular element with 9 degrees of freedom [7]–[10] was used. Fig. 1 shows a typical finite element idealization as used in the present study.

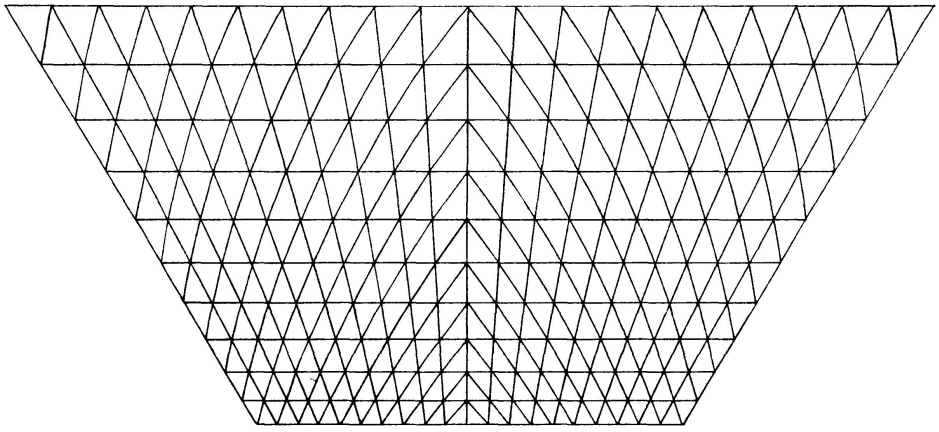

Fig. 1. A Typical Finite Element Idealization.

In what follows it is assumed that the diaphragm is composed of a homogeneous and isotropic material. Fig. 2 shows a typical trapezoidal diaphragm supported on two bearings. The parameters which influence the stress distribu-

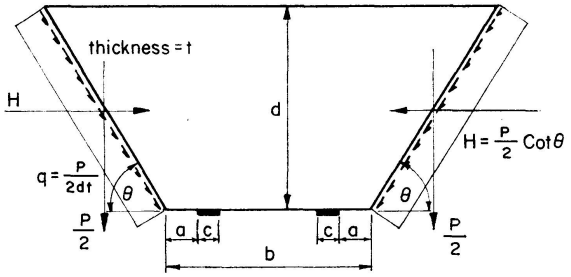

Fig. 2. Dimensions of a Typical Diaphragm.

tion and the buckling load are: the inclination of the webs (θ), the width to depth ratio of the diaphragm (b/d), the position and length of the bearings as defined by the parameters a/b and c/b, respectively. It has been assumed that the load is transmitted from the webs to the diaphragm by a uniform shear applied along the sides of the diaphragm. Two support conditions have been assumed, in the first, it is assumed that the load bearings are rigid in the vertical direction but do not prevent lateral movement, and in the second case (hereafter referred to as fixed supports) it is assumed that both horizontal and vertical displacements are prevented along the length of the bearings.

3. Results and Discussion

The study involved an examination of how the buckling load of the diaphragm varies with the following parameters:

1. The angle of slope of the web, θ.
2. The relative position of the supporting pads, a/b.
3. The relative width of the supporting pads, c/b.
4. The diaphragm aspect ratio, b/d.

3.1. Reactions

The distribution of the reaction forces will be seen to vary with the position of the pads and the results for six representative cases are shown in Fig. 3. The stress distribution in a diaphragm is effected by two actions which vary with the position and length of the bearings. First, when the bearing pads are "in set" as shown in Fig. 4a, there will be an overhanging moment which

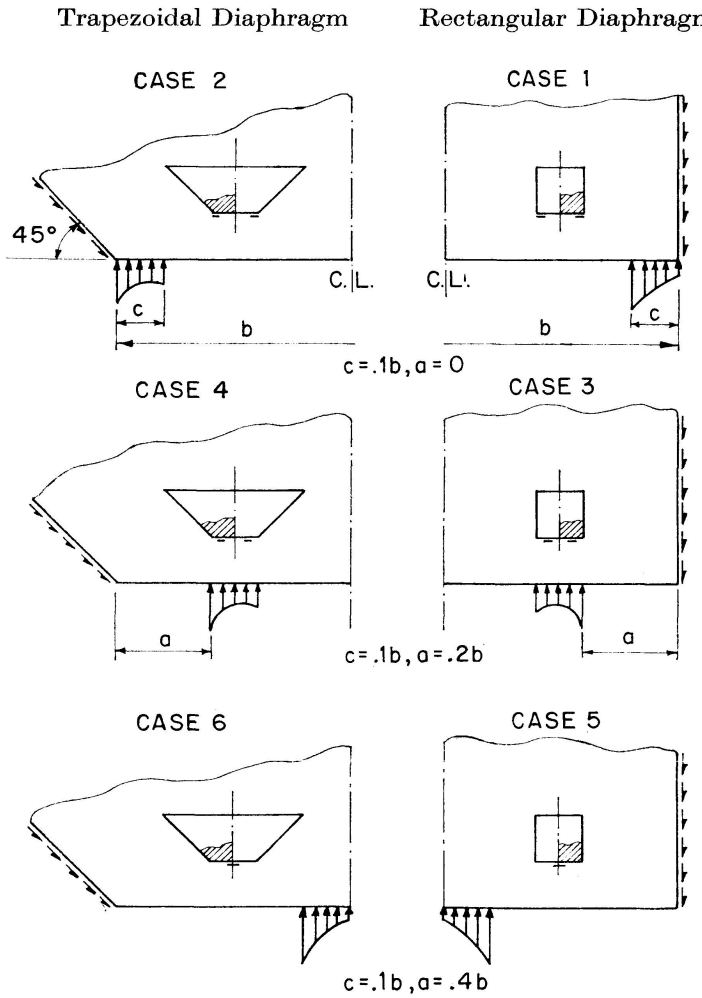

Fig. 3. Variation of the Distribution of the Reaction Forces with a Change in the Position of the Bearings, the Width of all the Bearings Being Constant ($= 0.1$ b) Diaphragms, $b/d = 1$.

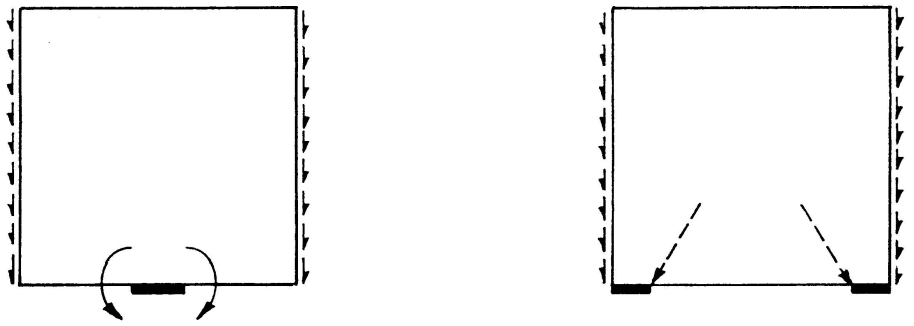

a) Overhanging Moment b) Arching Effect

Fig. 4. Overhanging Moment and Arching Effect.

becomes especially significant in the case of trapezoidal diaphragms. The second is an internal arching action as shown in Fig. 4b. Due to the arching effect the reactions must be larger at the inner edges of the pads whereas due to the overhanging moments, the reactions will be larger at the outer edges. In case 1, which is that of a rectangular diaphragm with a pad adjacent to the web, it will be noted from Fig. 3 that in the absence of any overhanging moment, the reactions are larger at the inner edges of the bearing pads and decrease gradually toward the outer edges. In cases 2, 3 and 4 due to the presence of both the arching effect and the overhanging moment the reactions are now larger at the two edges of the supporting pads. Finally, in the case of a central single pad, cases 5 and 6, due to the presence of a significant overhanging moment and the absence of any arching effect, the reactions are now very large at the outer edges of the pad and the variation of the reactions across the pad is quite rapid. Fig. 5 shows how the distribution of the reaction

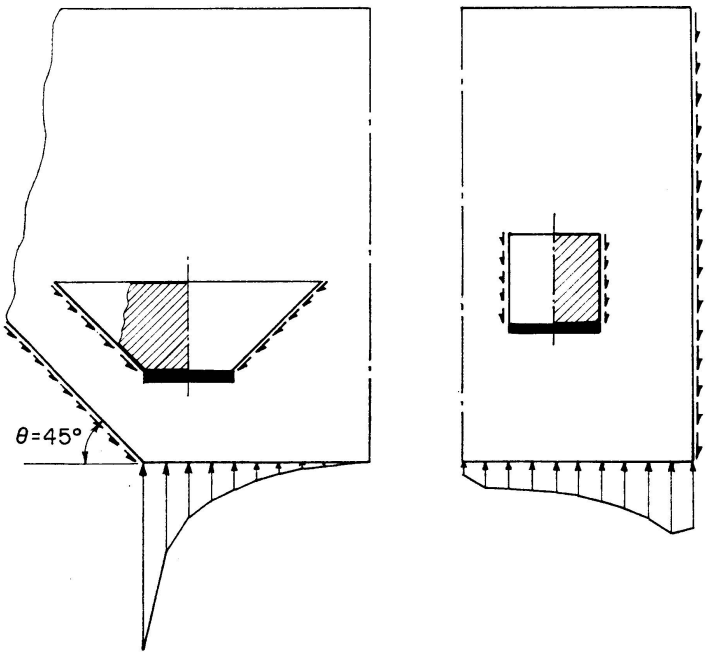

Fig. 5. Distribution of the Reaction Forces for a Continuous Supporting Pad ($c = b$).

forces varies when the supporting pad is continuous over the bottom width of the diaphragm, ($c = b$). In the case of the trapezoidal diaphragm the influence of the overhanging moment is shown to be significant.

3.2. Stresses

A diaphragm acts as a deep beam and therefore the simple theory of flexure cannot be used to determine the stress distribution within the diaphragm. Using a plane stress method of analysis, stress contours, of σ_x, σ_y and τ_{xy}, have been obtained for the 8 representative cases examined in Figs. 3 and 5, and are shown in Figs. 6, 7, 8 and 9. The stress values given were obtained when the diaphragm had the following dimensions and material properties: width (b) = 100″ (2450 mm), depth (d) = 100″ (2450 mm), thickness (t) = 0.125″ (3.175 mm), load (P) = 200 kips (90.72 tons), Young's modulus (E) = 29,000 ksi (2039 t/cm^2), and Poisson's ratio (μ) = 0.3.

3.2a. Stresses in the x-Direction σ_x

It will be seen that in all cases the horizontal stresses (σ_x) which are set up in the trapezoidal diaphragms are much larger than those occurring in the rectangular diaphragms due to the larger overhanging moment and the horizontal component of the shear. It will also be noted that the position of the supporting pads affects the magnitude of these stresses, since by moving the supporting pads toward the edges, the overhanging moment is reduced. Comparison between the values of σ_x obtained using the finite element method with values obtained using the elementary beam theory shows reasonable similarity for high aspect ratio b/d, see Fig. 10.

3.2b. Stresses in the y-Direction σ_y

These stresses are localized near the applied edge loads and the reactions, where they can reach very high values. As will be seen from Figs. 6, 7 and 8, the magnitude of σ_y does not vary significantly with the position of the supporting pad or the slope of the web, but does vary markedly with the width of the supporting pad, as shown in Fig. 9. It should be noted that these stresses do not decrease linearly with the increase in the width of the supporting pad, because of the concentration of the reaction forces near the edges of the supporting pad. In Fig. 11, the stress distribution of σ_y at the critical section (the edge of the supporting pad) is shown for three values of the c/b ratio.

3.2c. Shear Stresses τ_{xy}

In the neighbourhood of a concentrated load, localized shear stresses are always present and this is clearly shown in Figs. 6, 7 and 8. These very high local shear stresses occur in the same region as the high σ_y and σ_x values and clearly the stability of diaphragms in the neighbourhood of support bearings

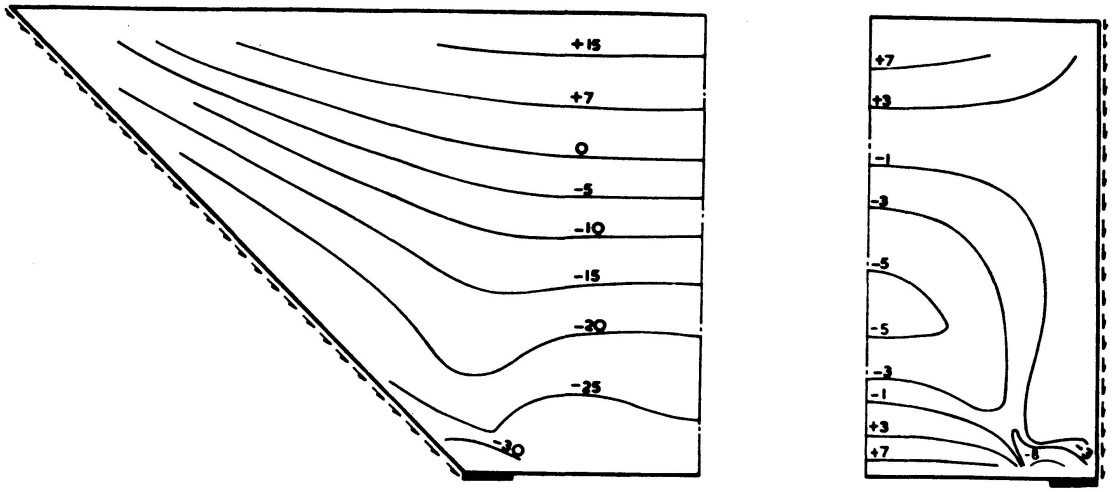

Stresses in the x-direction σ_x

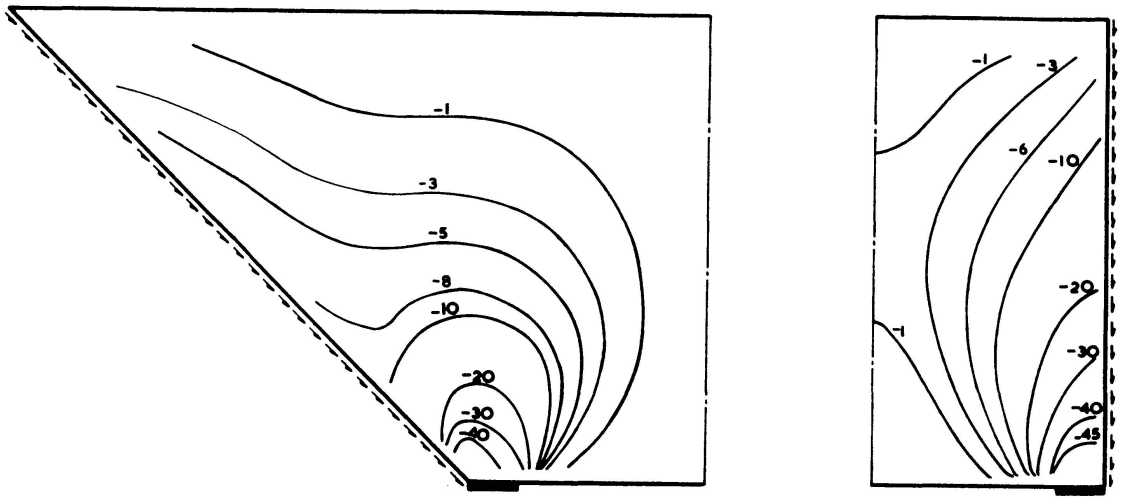

Stresses in the y-direction σ_y

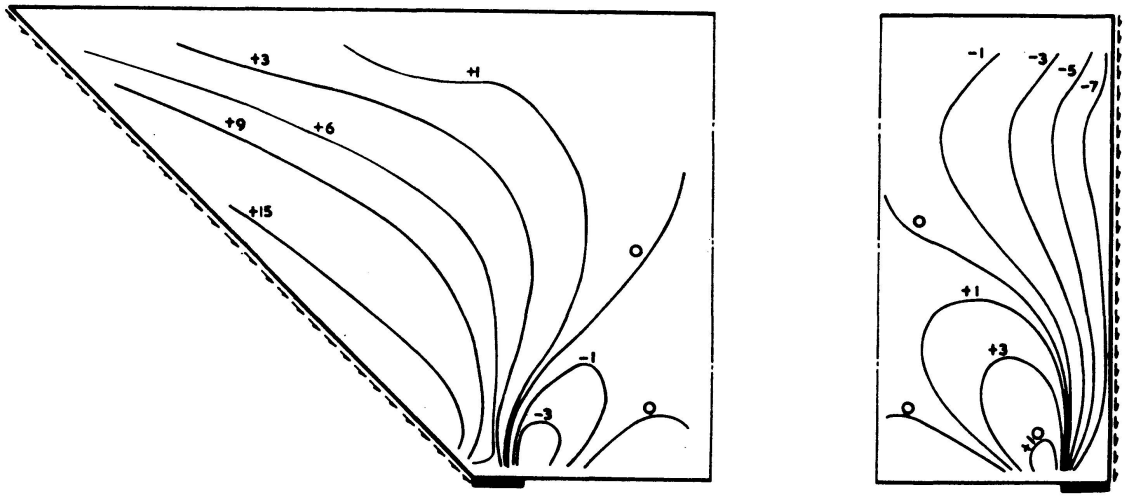

Shear stresses τ_{xy}

Fig. 6. Stresses σ_x, σ_y and τ_{xy} (Ksi).

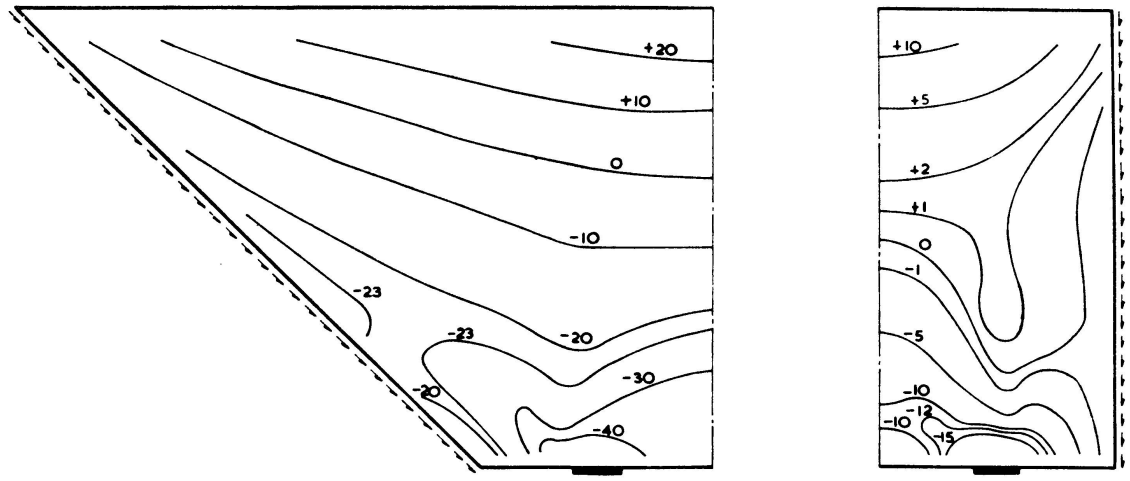

Stresses in the x-direction σ_x

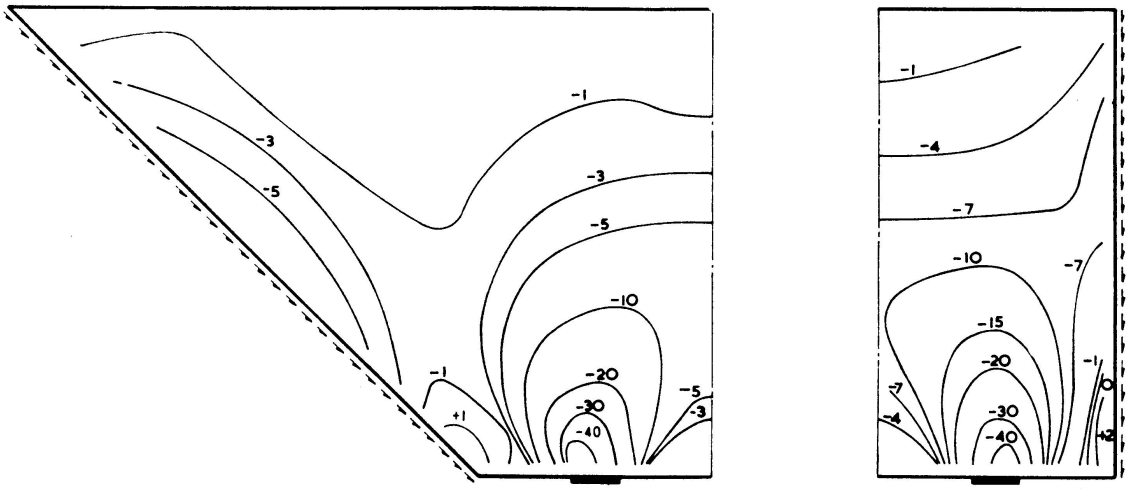

Stresses in the y-direction σ_y

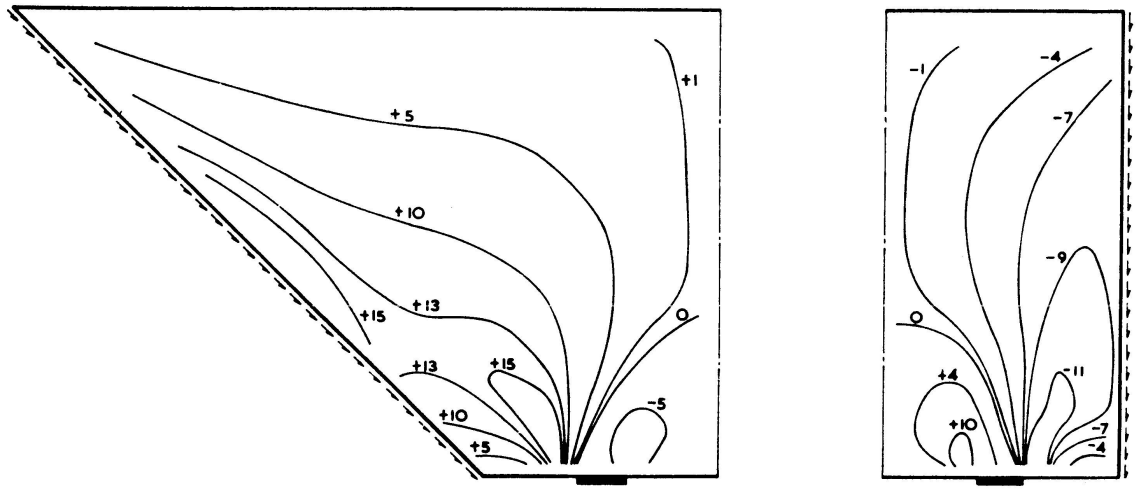

Shear stresses τ_{xy}

Fig. 7. Stresses σ_x, σ_y and τ_{xy} (Ksi).

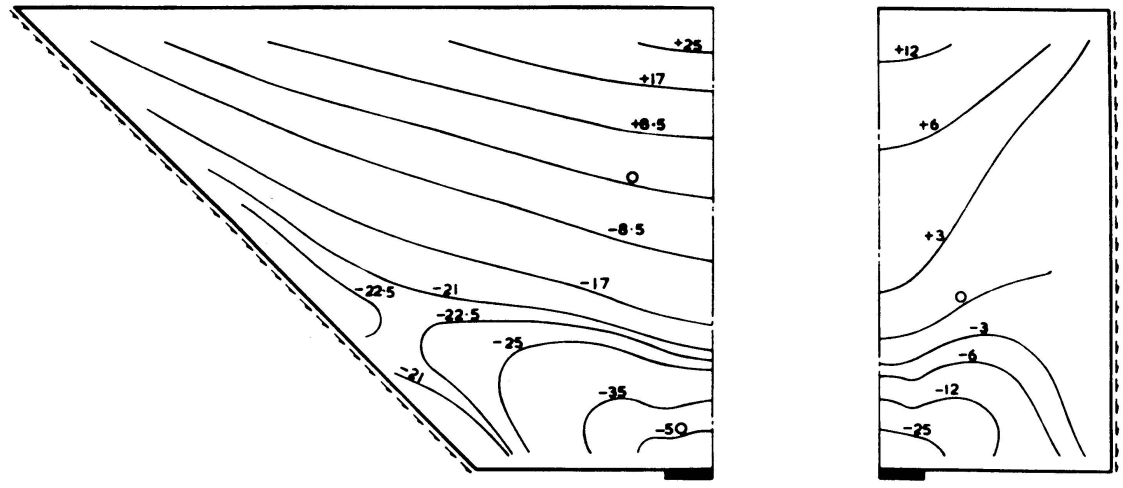

Stresses in the x-direction σ_x

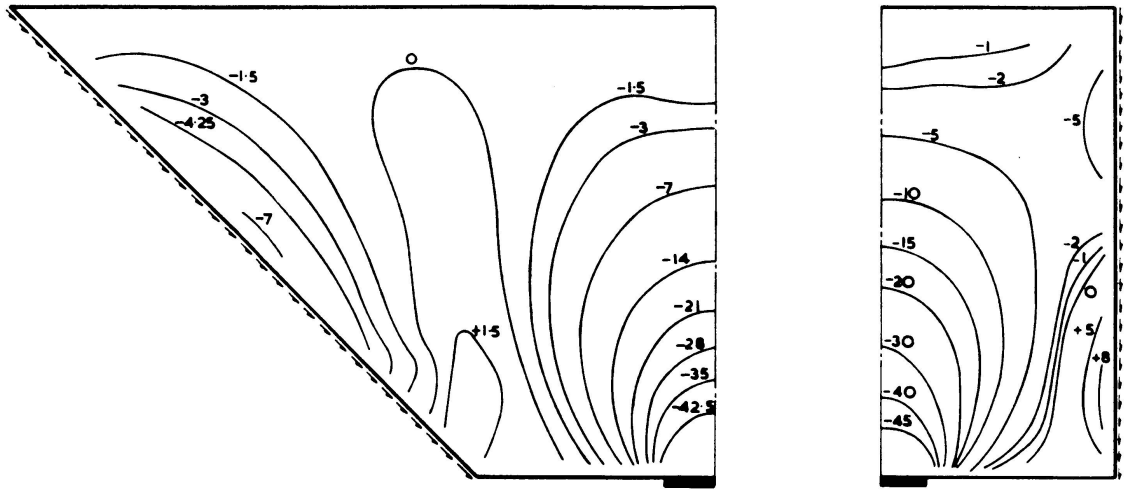

Stresses in the y-direction σ_y

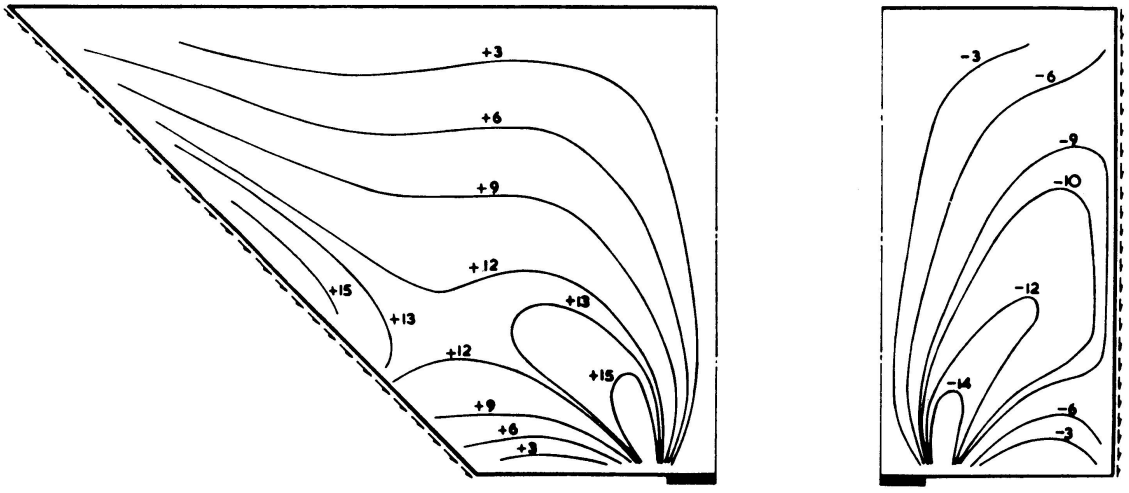

Shear stresses τ_{xy}

Fig. 8. Stresses σ_x, σ_y and τ_{xy} (Ksi).

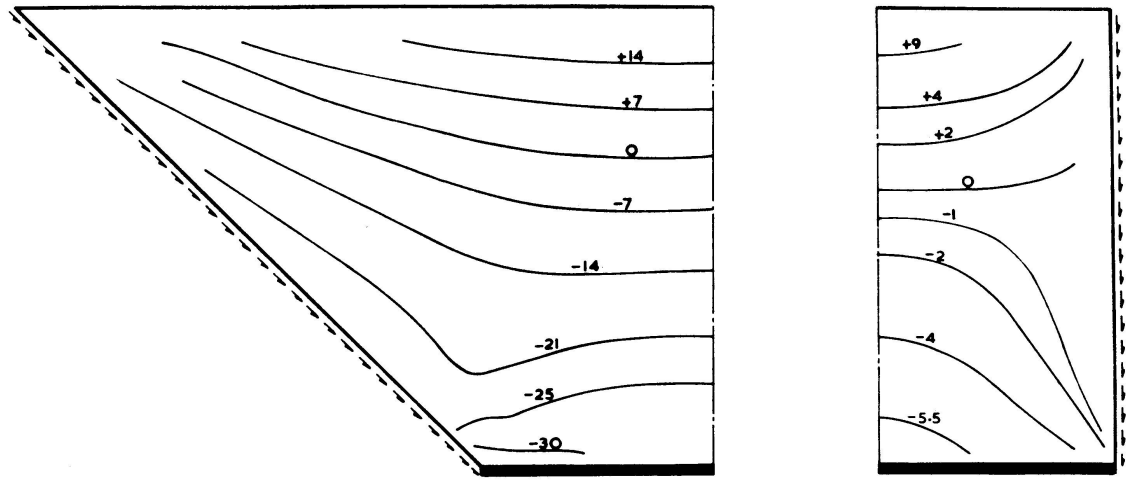

Stresses in the x-direction σ_x

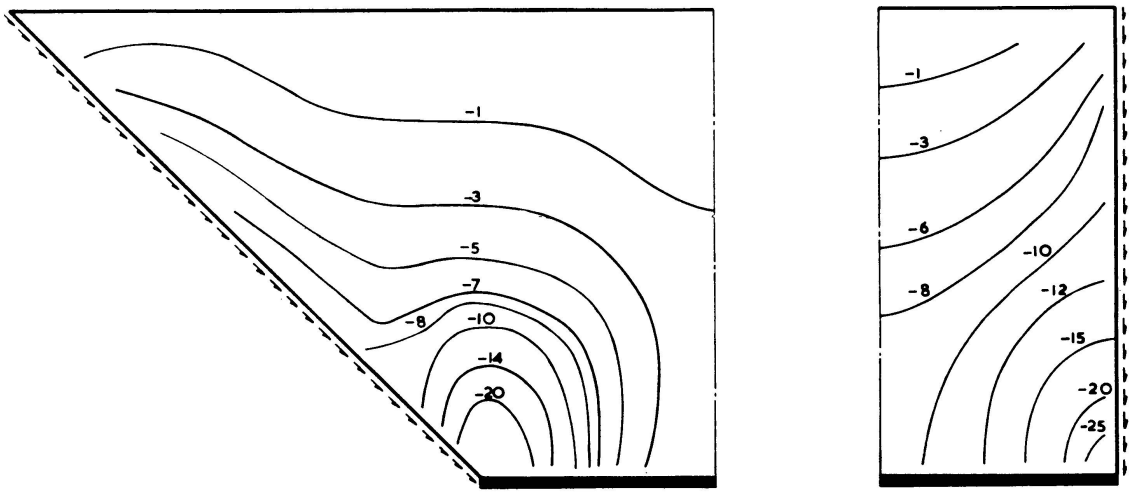

Stresses in the y-direction σ_y

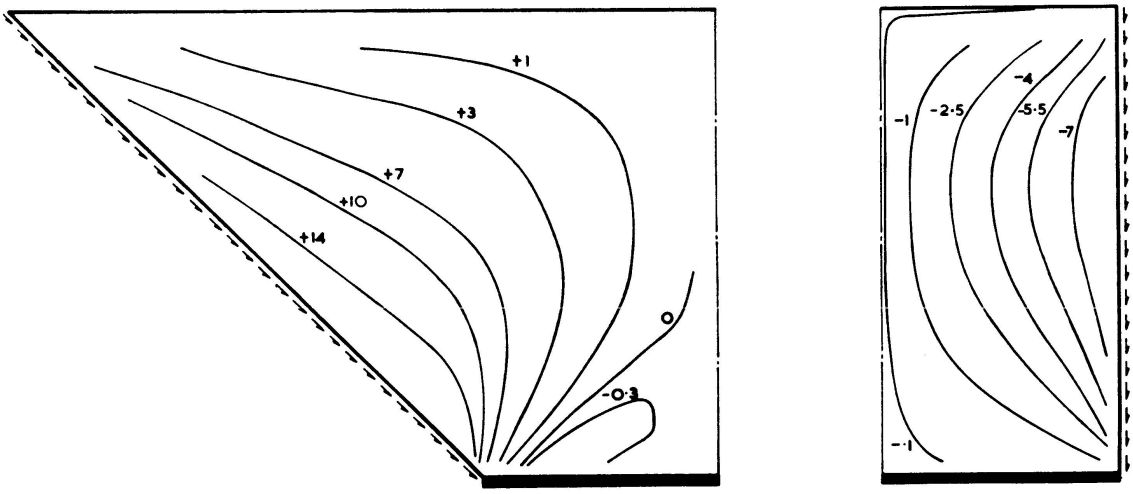

Shear stresses τ_{xy}

Fig. 9. Stresses σ_x, σ_y and τ_{xy} (Ksi).

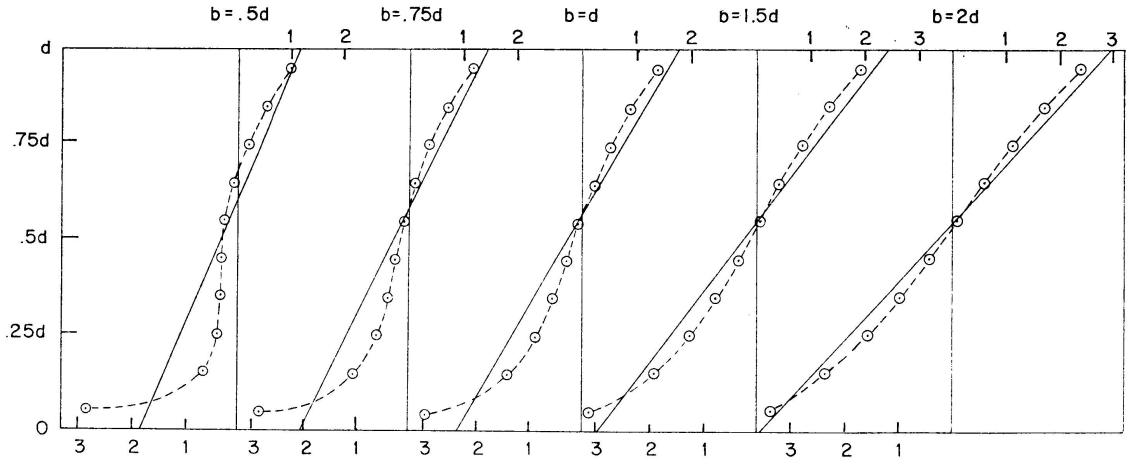

Central Supporting Pad ($c = 0.2b$, $a = 0.4b$) $\theta = 60°$

Fig. 10. Stresses σ_x Across the Depth at the Edge of the Supporting Pad – Comparison with Elementary Beam Theory.

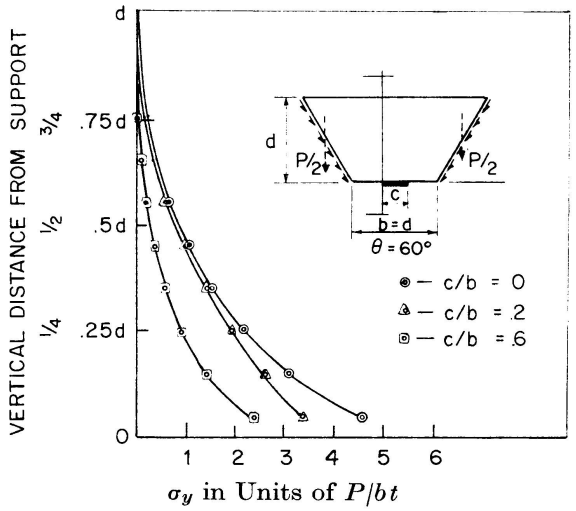

Fig. 11. Stress Distribution of σ_y at Critical Section.

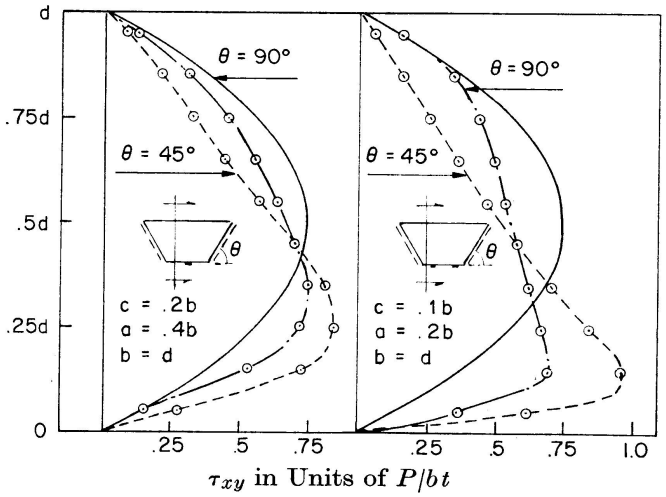

Fig. 12. Shear Stress Distribution Across the Depth.

needs special attention. Fig. 12 shows the shear stress distribution which occurs at a section midway between the outer edge of the supporting pad and the bottom corner of the diaphragm, for four representative cases. It will be noted that this shear stress distribution differs radically from the conventional parabolic form, the shear stresses in the lower portion being significantly greater than those acting in the upper portion of the diaphragm. Finally, one has to notice the localized shear stresses of opposite sign in the vicinity of the inner edges of the supporting pads, these stresses are induced since the total shear force between the inner edges of the pads is equal to zero.

3.3. Fixed Supports

The effect of preventing any horizontal movement along the length of the supporting pad has been examined. The σ_x, σ_y and τ_{xy} stress distributions which occur at representative sections are shown in Fig. 13, together with the corresponding stress distributions, which occur when horizontal movement along the length of the supporting pad is permitted (moveable supports). Clearly, the horizontal reactive forces at the two supports must be equal in magnitude and opposite in direction, and they induce localized tensile horizontal stresses (σ_x) between the inner edges of the supporting pads and additional localized compressive horizontal stresses outside the outer edges of the supports, as shown in Fig. 13. The effect on σ_y and τ_{xy} is also localized near the supports and is not as significant as the effect on σ_x.

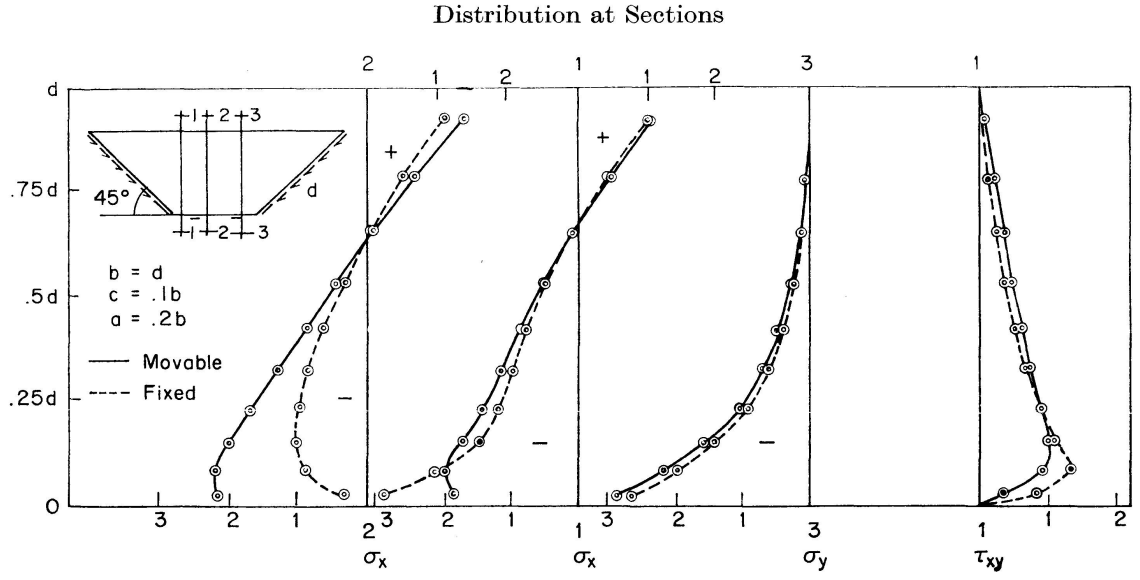

Fig. 13. The Effect of Preventing any Horizontal Movement Along the Length of the Supporting Pad on the σ_x, σ_y and τ_{xy} Stress Distributions.

3.4. General

In most practical cases the depth of the diaphragm (d) is comparable to its width (b), and hence the simple theory of flexure is not applicable. Consequently, the finite difference or the finite element method has to be used to solve the plane stress problem. In both methods difficulties will arise where steep stress gradient exists, hence the results obtained from both methods in the vicinity of concentrated loads (or reactions) are not dependable unless a very fine mesh is employed.

Fortunately, the stresses are linear functions of the term $\frac{P}{b\,t}$, thus the values given in this paper can be used for other values of P, b and t provided that the corresponding values of the parameters θ, a/b, c/b and b/d are identical.

3.5. Overall Buckling of Plane Simply Supported Diaphragms

In this section the buckling of a plane, unreinforced, trapezoidal diaphragm simply supported along its boundary will be considered.

Earlier work [11] on the buckling of rectangular web plates subjected to inplane patch loading has shown that the buckling load P_{cr} can be expressed by Eq. (1)

$$\frac{P_{cr}}{b\,t} = K \frac{\pi^2 E}{12\,(1-\mu^2)} \left(\frac{t}{d}\right)^2, \tag{1}$$

in which the non-dimensional parameter K is a function of the aspect ratio b/d and the width of the patch load c/b, see Fig. 14. Although the curves presented in Fig. 14 are not strictly applicable to the present problem, one would expect rather similar behaviour.

The overall buckling load P_{cr} for the trapezoidal diaphragm can be expressed

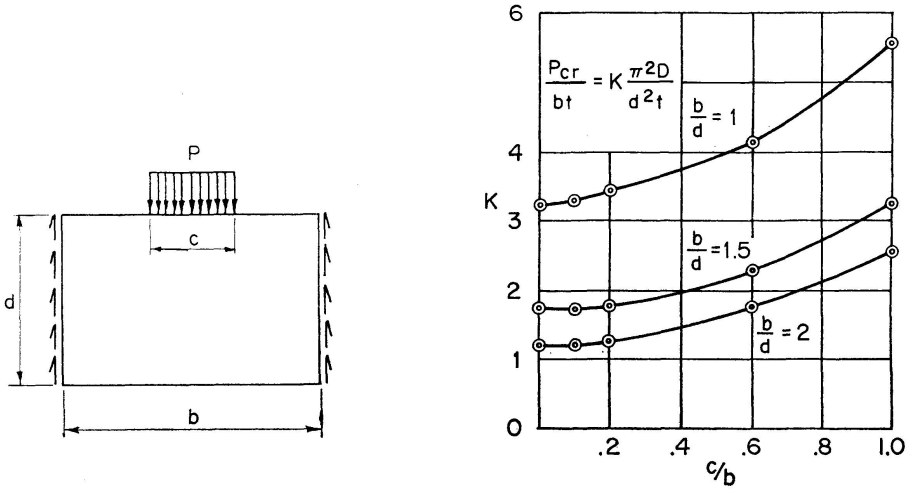

Fig. 14. Buckling Load Coefficient for Rectangular Web Plates Subjected to In-Plane Patch Loading (Reference 11).

in a similar form by Eq. (2)

$$\frac{P_{cr}}{dt} = K \frac{\pi^2 E}{12\,(1-\mu)^2}\left(\frac{t}{d}\right)^2, \tag{2}$$

in which the non-dimensional parameter K is a function of θ, a/b, c/b and b/d. Fig. 15 gives the results obtained for a diaphragm having an aspect ratio $b/d = 1.0$ and which is supported on non-yielding bearings of width $c = 0.1\,b$. The diaphragm is assumed to be simply supported on all four edges and to be subjected to a uniformly applied shear load along its "vertical" boundaries.

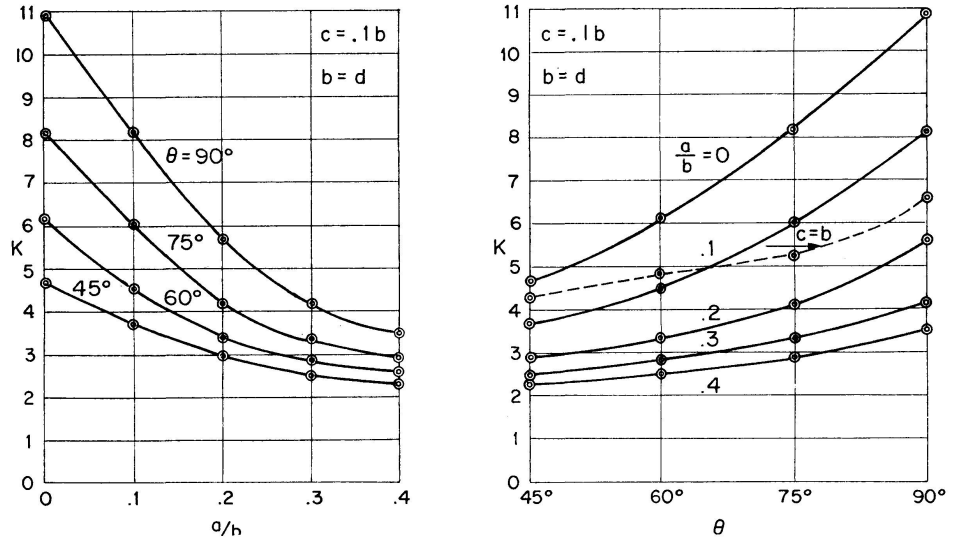

Fig. 15. Buckling Load Coefficient for Various a/b and θ Values ($b = d$, $c = 0.1b$).

It will be noted that the buckling coefficient K varies significantly with the angle of inclination θ of the sloping face, the reduction in values of the buckling coefficient K, with decreasing values of θ is due to the greater horizontal stresses induced into the web by the inclined forces. It will also be noted that the buckling coefficient K decreases as the pads are moved towards the centre of the panel. It will be recalled that the horizontal compressive stresses increase when the pads are moved away from the corners due to the influence of the overhanging moments. The effect of the position of the supporting pad on K is seen to be of increasing significance with increasing values of θ and is a maximum when $\theta = 90°$, since in this case the overhanging moment depends only on the position of the supporting pad. For smaller values of θ, a big overhanging moment as well as a horizontal component H are present even for $a/b = 0$, hence, increasing a/b will only increase the already existing moment and the decrease in K is therefore more gradual.

The dotted curve, in Fig. 15, is for the case of a continuous support along the bottom edge of the diaphragm. For high values of θ, the overhanging moment is small and consequently the reaction concentration near the edges

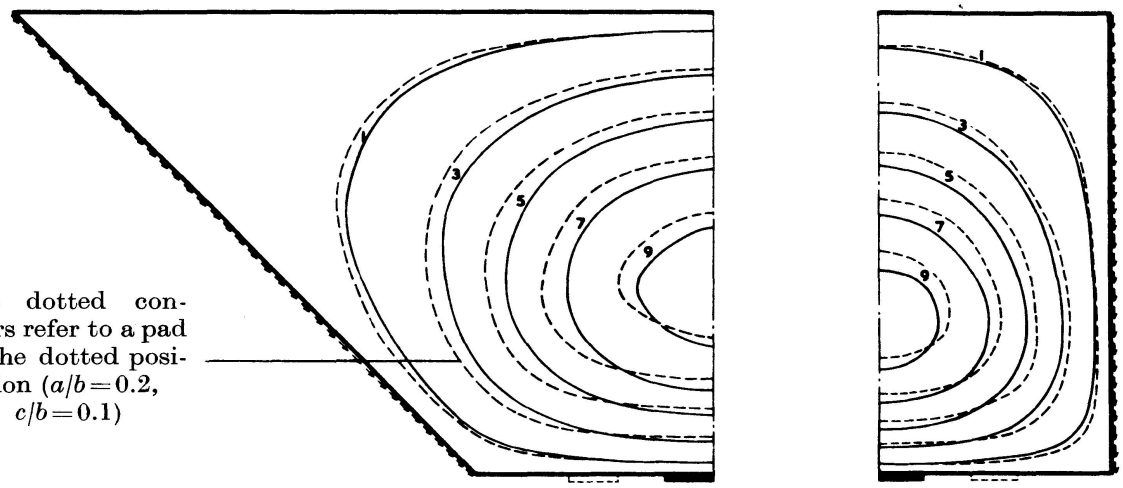

Supporting pads at $a/b=0.4$ and $c/b=0.2$

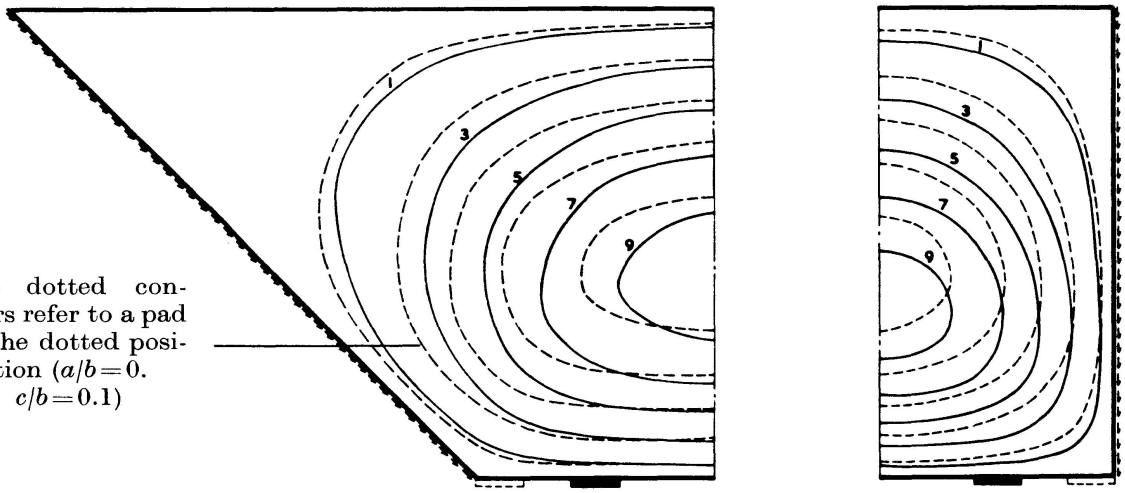

Supporting pads at $a/b=0.2$ and $c/b=0.1$

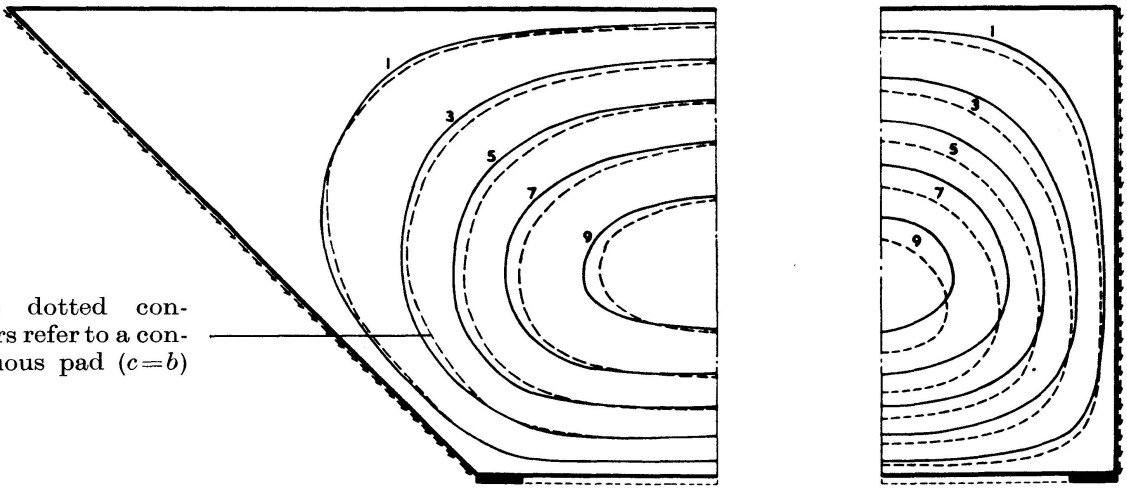

Supporting pads at $a/b=0$ and $c/b=0.1$

Fig. 16. Buckling Modes.

is relatively small and the buckling load is somewhere between the values for $a/b = 0.1$ and 0.2, however, for small values of θ the reaction concentration near the edges is higher and the buckling load is between the values for $a/b = 0$ and 0.1.

The buckling modes for six representative cases are shown in Fig. 16. In all cases it will be noted that there is a single half-wave buckling mode and that the crest of the half wave is nearer to the mid-depth position for lower values of θ due to the presence of the horizontal force H which elevates the position of the neutral axis. As mentioned before, there is an arching effect between the inner edges of the supporting pads which creates tensile stresses in the lower portion of the diaphragm which reduces the compressive stresses from the overhanging moment and the horizontal force. Therefore, the crest of the half wave moves upward by moving the supporting pads outward.

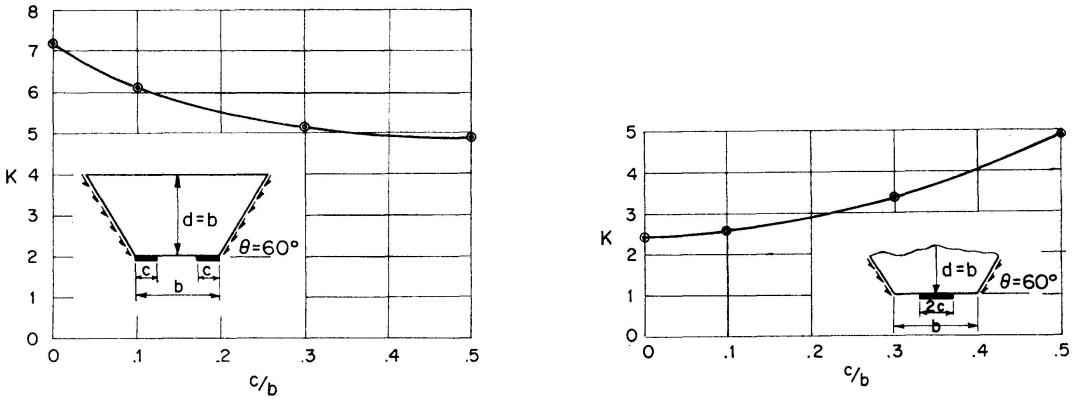

Fig. 17. Buckling Load Coefficient for Various c/b Values ($b = d$, $\theta = 60°$).

Fig. 17 shows how the buckling load of a trapezoidal diaphragm varies with the width of the supporting pad. In the case of two edge supporting pads, the buckling load is decreased by increasing the width of the pad. This is because the high values of the vertical stress σ_y, now act further away from the supported edges and in addition there will be less arching effect and consequently greater compression in the lower portion of the diaphragm. Meanwhile for a central supporting pad, the buckling load increases by increasing the width of the pad. The reason for this is obvious, since a wider supporting pad results in a smaller overhanging moment with a corresponding reduction in the horizontal stress σ_x whilst there is also a reduction in the vertical stress σ_y.

Finally, fig. 18 shows how the buckling coefficient K varies with the aspect ratio b/d for a representative case, in which the webs are inclined at 60° and the central pad has a width of $0.2b$. It will be noted that the relationship between the buckling coefficient K and the aspect ratio b/d is of a form very similar to that encountered in the compressive buckling of rectangular plates.

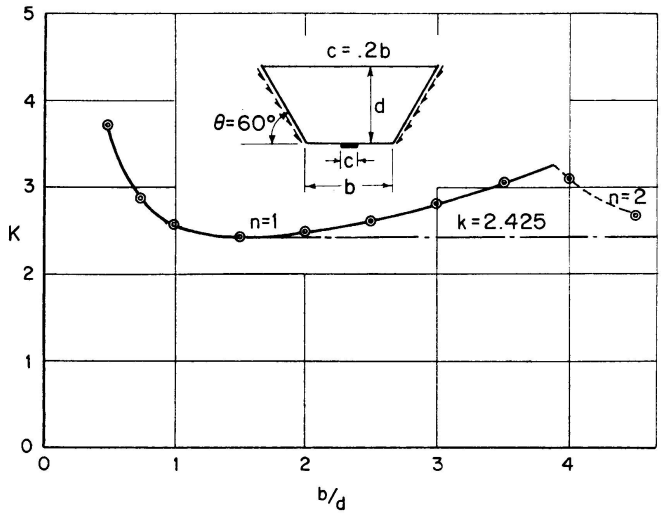

Fig. 18. Buckling Load Coefficient for Various b/d Values ($\theta = 60°$, $c/b = 0.2$, $a/b = 0.4$).

4. Conclusions

When the depth of the diaphragm is comparable to its width, the simple theory of flexure cannot be applied to determine the stress distribution within the area of the diaphragm. Moreover, the simple theory of flexure takes no account of the normal stresses in the y-direction, σ_y. In the present paper the stress distribution has been obtained, using the finite element method of analysis, for several representative cases. It has been found that the stress distribution varies with the inclination of the webs, the position and width of the supporting pads, and the aspect ratio of the diaphragm.

The overall buckling load has been determined for different geometric properties of the diaphragms and for varying position and length of the supporting pads, again using the finite element method of analysis. The buckling load has been expressed in the usual form for specifying critical loadings on flat plates. The non-dimensional buckling parameter K has been given as a function of θ, a/b, c/b and b/d.

Notation

a Distance between the bottom corner of the diaphragm and the outer edge of the supporting pad (see Fig. 2).
b Width of the bottom edge of the diaphragm.
c Width of the supporting pad.
d Depth of the diaphragm.
E Young's modulus of elasticity.
K Non-dimensional buckling coefficient.
P Applied total vertical load.

P_{cr} Critical buckling load.
t Thickness of the diaphragm.
θ Angle of inclination of the web.
μ Poisson's ratio.
σ_x Normal stresses in the horizontal direction.
σ_y Normal stresses in the vertical direction.
τ_{xy} Shear stresses.

References

1. Turner, M. J., Clough, R. W., Martin, H. C. and Topp, L. J.: Stiffness and Deflection Analyses of Complex Structures. Journal of Aeronautical Sciences, Vol. 23, No. 9, September, 1956, p. 805.
2. Clough, R. W.: The Finite Element Method in Plane Stress Analysis. 2nd Conference on Electronic Computation, Pittsburgh, Pa. Sept. 8–9, 1960. Sponsored by the ASCE.
3. Kapur, K. K., and Hartz, B. J.: Stability of Plates Using the Finite Element Method. Proc. ASCE, Jour. of Eng. Mech. Div., Vol. 92. No. EM 2, April 1966, pp. 177–195.
4. Bagchi, D. K.: Large Deflection and Stability of Structural Members using the Finite Element Method. Ph. D., thesis, University College, Cardiff, 1969.
5. Clough, R. W.: The Finite Element Method in Structural Mechanics. Stress Analysis, edited by O. C. Zienkiewicz and G. S. Holister. Jon Wiley & Sons Ltd., London-New York-Sydney, 1965.
6. Argyris, J. H.: Recent Advances in Matrix Methods of Structural Analysis. Pergamon Press, Oxford, 1964.
7. Zienkiewicz, O. C.: The Finite Element Method in Structural and Continuum Mechanics. McGraw-Hill, London, 1967.
8. Bazeley, G. P., Cheung, Y. K., Irons, B. M. and Zienkiewicz, O. C.: Triangular Elements in Plate Bending – Conforming and Non-Conforming Solutions. Matrix Methods in Structural Mechanics, Proceedings of the Conference held at Wright-Patterson Air Force Base, Ohio 1965 (Editor J. S. Przemieniecki).
9. Clough, R. W. and Tocher, J. L.: Finite Element Stiffness Matrices for Analysis of Plate Bending. The same book as Reference 8.
10. Argyris, J. H.: Matrix Displacement Analysis of Anisotropic Shells by Triangular Elements. J. of the Royal Aeronautical Society, Vol. 69, Nov. 1965.
11. Rockey, K. C., and Bagchi, D. K.: Buckling of Plate Girders Webs under Partial Edge Loadings. Int. J. Mech. Sci. Pergamon Press 1970, Vol. 12, pp. 61–76.

Summary

In this paper, the finite element method of analysis has been used to determine the stress distribution which occurs in both rectangular and trapezoidal diaphragms and to determine the applied load at which overall buckling of the diaphragms will occur. Stress contours have been given for various representative cases and the effect of the geometric properties of the

diaphragms and the position and length of the supporting pads has been examined. The buckling load has been expressed in the usual form for specifying critical loadings on flat plates and the non-dimensional buckling coefficient K has been given as a function of the parameters involved.

Résumé

La méthode des éléments finis a été utilisée pour déterminer la distribution des tensions dans les entretoises transversales, rectangulaires ou trapézoidales et la charge de voilement. On examine la distribution des tensions pour différents cas ainsi que l'influence des dimensions des entretoises et de la disposition et de la longueur des dalles d'appuis. La charge de voilement est exprimée sous la forme usuelle pour les charges critiques des plaques minces. Le coefficient de voilement K non-dimensionnel est donné en fonction des paramètres impliqués.

Zusammenfassung

Die Methode der finiten Elemente wurde verwendet, um die Spannungsverteilung, welche in rechteckigen und trapezförmigen Querträgern auftritt, sowie die kritische Beullast zu bestimmen. Die Spannungsverteilung wird für verschiedene repräsentative Fälle angegeben. Der Einfluss der geometrischen Abmessungen der Querwände sowie verschiedener Anordnungen und Längen der Auflagerplatten wurde ebenfalls untersucht. Die Beullast ist in der gleichen Form wie bei dünnen Platten ausgedrückt, und der dimensionslose Beulwert K wird in Funktion der verwendeten Parameter angegeben.